INORGANIC CHEMISTRY
FRONTIERS

RESEARCH ARTICLE

View Article Online
View Journal | View Issue

Cite this: *Inorg. Chem. Front.*, 2017, **4**, 1281

Ferroelectricity in bis(ethylammonium) pentachlorobismuthate(III): synthesis, structure, polar and spectroscopic properties†

Anna Piecha-Bisiorek,*[a] Anna Gągor,[b] Ryszard Jakubas,[a] Agnieszka Ciżman,[c] Rafał Janicki[a] and Wojciech Medycki[d]

Received 9th May 2017,
Accepted 1st June 2017

DOI: 10.1039/c7qi00254h

rsc.li/frontiers-inorganic

A brief description of the thermal, structural and dielectric properties of bis(ethylammonium) pentachlorobismuthate(III) ferroelectric with P_s that equals to 1.4 μC cm^{-2} at 180 K is presented. This paper focuses in particular on the molecular mechanism of a phase transition that is related mainly to the deformation of the anionic sublattice confirmed by temperature-variable powdered UV-Vis spectroscopy.

Introduction

The conscious synthesis and design of organic–inorganic hybrid materials based on divalent or trivalent metal halides have attracted scientific attention not only due to their interesting structural topologies but also due to their unique chemical and physical properties as well as extremely useful applications in the areas of optoelectronics, data communication, switchable dielectric devices, and rewritable optical data storage.[1–4]

Haloantimonates(III) and halobismuthates(III) of the general formula $R_aM_bX_{3b+a}$ (where R is organic cations M = Sb, Bi and X = Cl, Br, I) constitute an important class of functional materials characterized by a number of interesting electrical/ferroelectric, elastic/ferroelastic and nonlinear optical (NLO) properties and act as potential lead-free absorber materials for solar cells.[5–12] Numerous structural studies have shown that Sb^{III}/Bi^{III} halide derivatives based on different organic amines exhibit a rich diversity of the anionic structures.[13,14] These systems usually consist of zero- (0D), one- (1D), two- (2D) and rarely three-dimensional (3D) inorganic networks. It has turned out that an especially promising electric (ferroelectric) response is encountered in the selected anionic species *e.g.* $[M_2X_{11}]^{5-}$ (0D), $[MX_5]^{2-}$ (1D), $[MX_4]^{-}$ (1D) and $[M_2X_9]^{3-}$ (2D). In the compounds with the $R_3M_2X_9$ chemical composition, polar properties have been found in the system, where R stands for small alkylammonium cations as: $CH_3NH_3^+$,[15–18] $(CH_3)_2NH_2^+$ (ref. 19–21) or $(CH_3)_3NH^+$.[22,23] As regards $R_5M_2X_{11}$-type compounds, it is interesting that all known and characterized compounds crystallizing with this composition (like methylammonium,[24,25] pyridinium[26] and imidazolium[27–29] analogs) exhibit ferroelectric properties. It should be underlined that the paraelectric–ferroelectric phase transitions (PTs) found in $R_3M_2X_9$ and $R_5M_2X_{11}$ type derivatives have been explained in terms of an 'order–disorder' mechanism, where the dipolar organic cation dynamics seems to play a crucial role.[14]

In recent years, the research on nonlinear organic–inorganic hybrids gained new impetus with the discovery of ferroelectricity within haloantimonates(III) and halobismuthates(III) crystallizing with the chemical stoichiometry: R_2MX_5.[5–10] It should be stressed that for this composition only three ferroelectrics have been reported so far, $(MV)BiBr_5$ (where MV^{2+} is methylviologen dication) with the *trans* configuration of the $[MX_5]^{2-}{}_\infty$ chains, $(H_2dmdap)SbCl_5$ (dmdap = *N*,*N*-dimethyl-1,3-diaminopropane) and $(C_3N_2H_5)_2SbCl_5$ (imidazolium cation) with the *cis* modification of the $[MX_5]^{2-}{}_\infty$ chains.[5,6,10] The ferroelectric PTs taking place in $(MV)BiBr_5$ and $(H_2dmdap)SbCl_5$ are connected mainly to a significant distortion of regular *trans*- and *cis*-connected octahedra ('displacive' contribution), leading to strong polar polyanionic substructures.[5,6] Moreover, the Bi^{3+} $(6s^2)$ and Sb^{3+} $(5s^2)$ electronic lone pairs are stereochemically activated below 243 and 143 K, respectively, which contributes additionally to the polar properties of the low temperature phases. In the case of $(C_3N_2H_5)_2SbCl_5$ ferroelectric, the molecular mechanism of the paraelectric–ferroelectric PT is more complex and related to

---

[a] *Faculty of Chemistry, University of Wrocław, F. Joliot-Curie 14, 50-383 Wrocław, Poland. E-mail: anna.piecha@chem.uni.wroc.pl*
[b] *W. Trzebiatowski Institute of Low Temperature and Structure Research PAS, P.O. Box 1410, 50-950 Wrocław, Poland*
[c] *Institute of Physics, Wrocław University of Technology, Wybrzeże Wyspiańskiego 27, Wrocław, Poland*
[d] *Institute of Molecular Physics, Polish Academy of Science, Smoluchowskiego 17, 60-179 Poznań, Poland*

† Electronic supplementary information (ESI) available: Details of the crystal structure, thermal and dielectric properties as well as proton magnetic resonance studies (^{1}H NMR). CCDC 1548779 and 1548780. For ESI and crystallographic data in CIF or other electronic format see DOI: 10.1039/c7qi00254h

the polar imidazolium cation dynamics ('order–disorder' part) as well as by an ability to induce polar polyanionic substructures ('displacive' participation).[10]

In this paper, we report the synthesis, crystal structures, dielectric and spectroscopic properties of a unique ferroelectric compound, bis(ethylammonium) pentachlorobismuthate(III), $(C_2H_5NH_3)_2BiCl_5$ (abbreviated as (**ECB**)). Herein, we will show that the compound under investigation experiences the PT related mainly to a significant deformation of the inorganic $[BiCl_5]^{2-}{}_{\infty}$ chains of *cis*-connected octahedra. A noteworthy is the fact that the 'displacive' component, responsible for the molecular mechanism of the ferroelectric PT, is not encountered in haloantimonates(III) and halobismuthates(III).

Results and discussion

ECB undergoes a reversible PT at 189.5/190 K (Fig. 1(a)) and exhibits thermal stability up to about 450 K (Fig. S2†). As one can see, it is difficult to define unequivocally the nature of the observed PT. On the one hand, the shape of the thermal anomaly and the presence of the thermal hysteresis (ΔT < 0.5 K) indicate a weak discontinuous nature of a low-temperature PT. On the other hand, the lack of the phase front suggests that we deal with the PT close to the second order type. The transition entropy (ΔS) was estimated to be 5.7 J mol^{-1} K^{-1} ($\approx R\ln 2$).

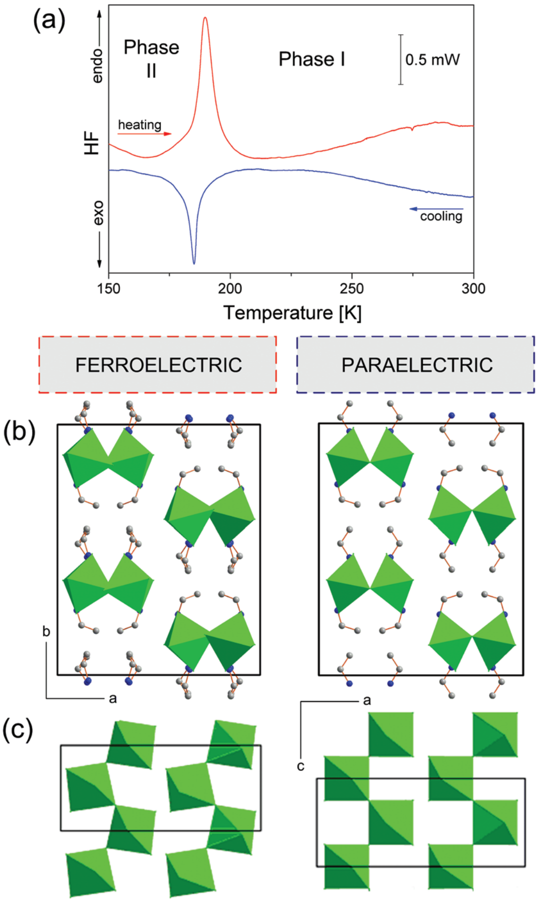

Fig. 1 (a) DSC data confirming the transition sequence seen in **ECB** (rate: 10 K min^{-1}, sample mass: 12.86 mg); (b) the structure overview of the paraelectric Phase I (right) and ferroelectric Phase II (left); (c) $[BiCl_5]^{2-}{}_{\infty}$ chains propagate along the *c*-direction and distinctly deform after the PT.

ECB crystallizes in the orthorhombic system, with *Acam* space group symmetry at room temperature (RT) (more in ESI, Part 3†). The inorganic substructure is built up of polymeric $[BiCl_5]^{2-}{}_{\infty}$ chains propagating along the *c*-axis (see Fig. 1(b) and (c), right). The elemental unit of each chain is the $BiCl_6$ octahedron, which at RT possesses C_s local symmetry. Neighbouring octahedra connect *via* two apexes forming zigzag structures also of C_s symmetry. There are three types of Bi–Cl bonds in the octahedra: bridging, terminal across from bridging and terminal across from the terminal. Due to the *trans* effect[30] that occurs in halobismuthates(III) and haloantimonates(III), the longest are the bridging bonds (2.841(1) Å), whereas the shortest are terminal across from bridging (2.577(2) Å). Terminal across from terminal bonds adopt the intermediate values of 2.676(1) and 2.688(2) Å. The closest Cl⋯Cl distances between the chains are equal to 4.117(1) Å. The ethylammonium counterions are embedded between the chains and interact *via* N–H⋯Cl hydrogen bonds with all terminal chlorine atoms. There are two symmetrically independent ethylammonium moieties at RT, A and B. Both are disordered over the ..m mirror plane and adopt two equivalent positions with the 0.5/0.5 occupancy ratio. Additionally, in Phase I, the hydrogen atoms from each NH_3 group are disordered into two equivalent positions, each with 50% occupancy. The positions are rotated by 60 degrees from one another. This disarray of hydrogen atoms enables them to form alternative hydrogen bonds with identical geometry. The NH_3 ammonium group of cation A forms hydrogen bonds between two neighbouring $[BiCl_5]^{2-}{}_{\infty}$ chains, whereas the NH_3 ammonium group of cation B interacts with chlorine ions from the same chain. Fig. 3(b) and (c) illustrate the atomic configuration around both ethylammonium ions together with N–H⋯Cl hydrogen bonds. Table S3† collects the geometry of hydrogen bonds at both phases.

The PT at 189.5 K is accompanied by the lowering of the space group symmetry to polar *Aba*2. The ..*m* mirror plane, which in Phase I had a great impact on the geometry of the inorganic anions and the arrangement of the organic cations, vanishes. This relieves the amines from a quite uncomfortable high symmetry placement, which inducted the disorder of hydrogen groups, and significantly alters the mutual orientation of $BiCl_6$ octahedra in the polymeric $[BiCl_5]^{2-}{}_{\infty}$ chains. The cations reorient in a manner which gives the best setting of NH_3 groups with respect to the new acceptor positions. The geometry of hydrogen bonds between both A and B groups and the chains improves significantly compared to the high-temperature setting. Each hydrogen atom has its chlorine acceptor; the donor to acceptor distances shorten and the donor to hydrogen to acceptor angles open more, see Table S3.† In the polar phase, the A ions are ordered, whereas the B ions are still disordered and accommodate two inequivalent positions with the 0.6/0.4 ratio at 100 K.

The dynamics of the ethylammonium cations in both phases is reflected in the dielectric measurements. As it is presented in Fig. 2(a), the real part of the complex electric permittivity measured between 10 Hz and 1 MHz for the polycrystalline sample shows a step-wise change at about 189.5 K upon cooling, being well consistent with that of DSC and further confirming the occurrence of a reversible PT (see also Part 4 in the ESI†). The dielectric constant displays a pronounced change up to about 19 around the paraelectric–ferroelectric PT above which ε' obeys the Curie–Weiss law (see Fig. S3†).

The linear part of the $1/\varepsilon'$ *vs.* temperature curve is maintained only over a narrow temperature region, of about 2 K above and 3 K below 189.5 K. No dielectric dispersion is visible in the paraelectric Phase I which means that the motion of the dipolar groups is relatively fast in the disordered Phase I. On the other hand, there is a clear low frequency relaxation process over Phase II, most probably, due to the motion of ferroelectric domain walls.

All the pieces of evidence point to a ferroelectric PT at 189.5 K in **ECB**, and indeed a ferroelectric hysteresis loop was recorded (Fig. 2(c)) using a home-made high precision set-up based on the Diamant–Drenck–Pepinsky (DDP) bridge at 50 Hz. Just below T_c, a typical ferroelectric hysteresis loop emerges (Fig. 2(c)), confirming the ferroelectricity of **ECB**. Fig. 2(d) shows the spontaneous polarization (P_s) which is estimated by means of the pyroelectric current measurements. P_s was found to be reversible in an external electric dc field (±5 kV $\mathrm{cm^{-1}}$). The value of P_s reaches *ca.* 1.4 μC $\mathrm{cm^{-2}}$ at 180 K.

Each ethylammonium cation possesses a permanent dipole moment. In the paraelectric Phase I (Fig. 3 (right)), the resultant dipole moment from all amines is equal to zero, due to the presence of the symmetry center. In Phase II (Fig. 3 (left)), the spatial arrangement of the ethylammonium dipole moments gives rise to the P_s along the *c* direction. The analysis of symmetry modes performed with the program AMPLIMODES[31] shows also that important impact on the PT have polar displacements of the inorganic part. The $[\mathrm{BiCl_5}]^{2-}{}_{\infty}$ chains experience a significant distortion as a result of the PT. The structure of Phase II has two distortion modes – a primary one that yields *Aba*2 symmetry and the secondary one that has the symmetry of the high-temperature phase *Acam*. The displacements of all chain atoms have the symmetry of the primary and secondary modes, with the primary mode dominating, and contribute to the P_s. The maximum atomic displacement in the distortion concerns bridging Cl(4) chlorine that shifts 0.59(1) Å. The total distortion amplitude that is given by the square root of the sum of the squares of all atomic displacements is equal to 1.64(1) Å. The details concerning the atomic displacements between the two phases are given in the ESI (Part 3.1†). The distortion amplitude of the primary mode is equal to 1.59(1) Å, while the amplitude of the secondary mode is much weaker, equal to 0.40(1) Å.

Taking into account the values of the distortion modes, **ECB** appears to be a ‘well-behaved’ ferroelectric, with the atomic displacements of the order of 0.5 Å, as in conventional ‘displacive’ ferroelectrics.[1]

Basic conclusion emerging from the structural analysis and concerning the change in the motional state of the ethyl-

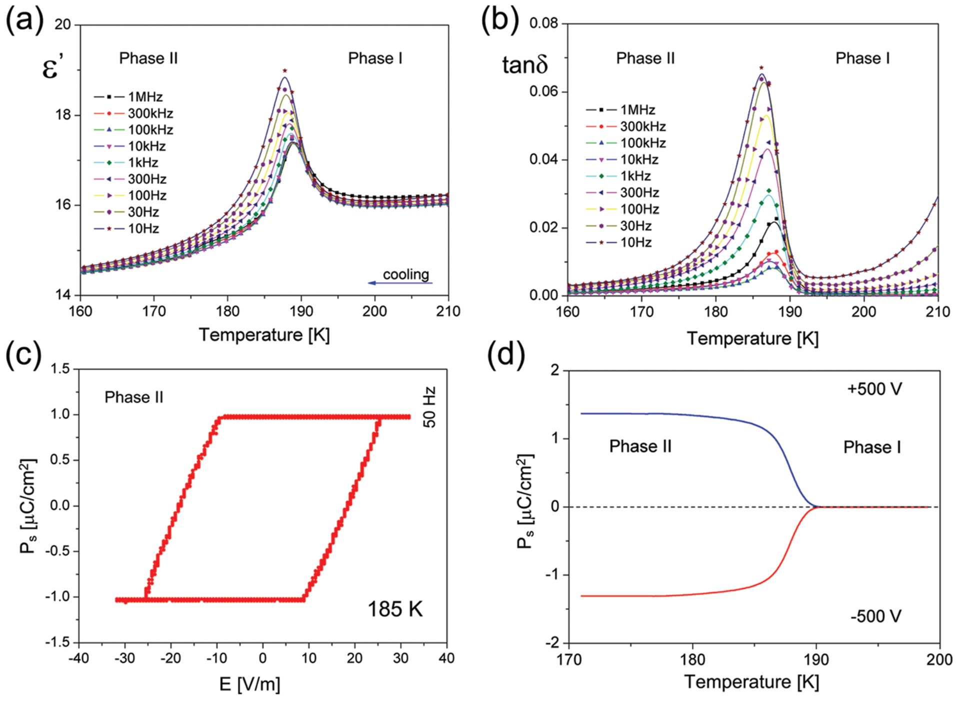

Fig. 2 (a, b) Dielectric properties of **ECB** measured at different frequencies as a function of temperature; (a) dielectric constant across the Curie point; (b) the imaginary part of the dielectric constant; (c) hysteresis loop measured at 185 K. (d) Spontaneous polarization *vs.* temperature.

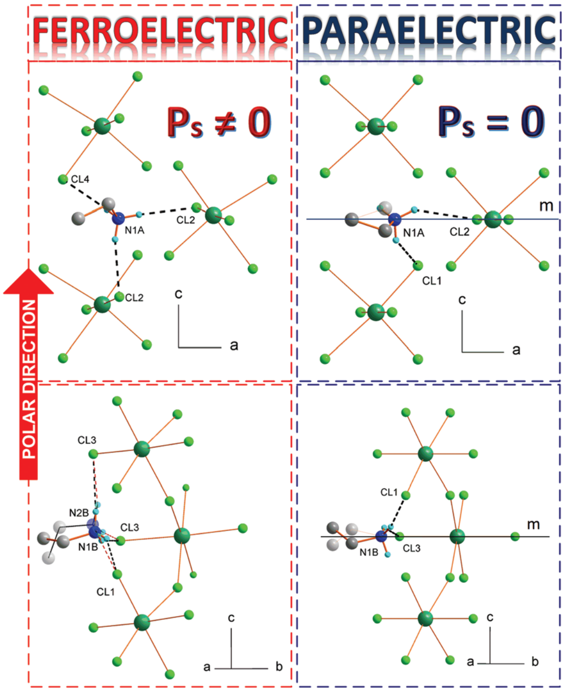

Fig. 3 The details of the cation arrangements in both phases. In paraelectric Phase I, both cations A and B are disordered over the ..m mirror plane with the 0.5/0.5 occupancy ratio; in ferroelectric Phase II, the A moiety is ordered, whereas the B takes two independent spatial orientations with the 0.6/0.4 occupancy ratio at 100 K. Dashed lines stand for hydrogen bonds.

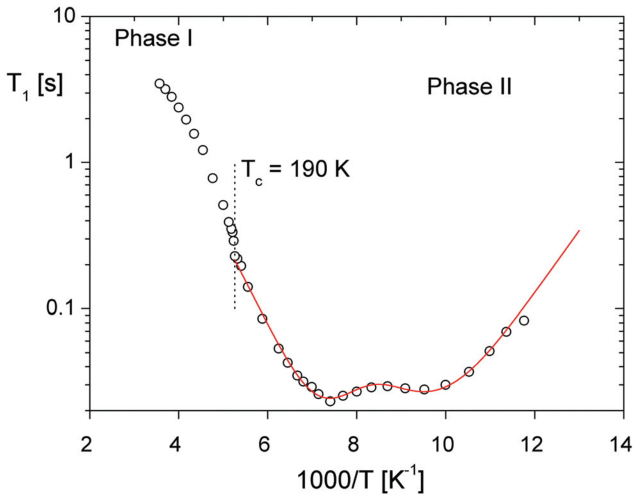

Fig. 4 Temperature dependence of the spin–lattice relaxation time (T_1) of ^{1}H NMR; the solid line represents the best fit calculated using eqn (1) in ESI, Part 5.†

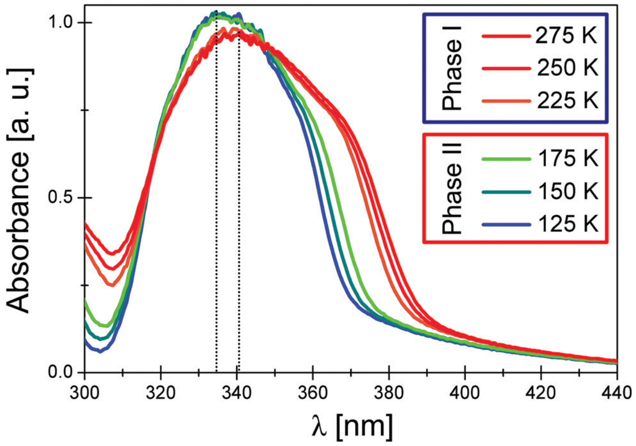

Fig. 5 UV-vis absorption spectra of the compound under study at different temperatures.

ammonium cations through the ferroelectric PT seems to correspond well with the ^{1}H NMR results presented in Fig. 4. As seen in this figure, the T_1 *vs.* T^{-1} curves are characterized by a double minimum of 23 ms at 135 K and 28 ms at *ca.* 105 K for the $C_2H_5NH_3^+$ ions. A careful analysis leads to the conclusion that these minima may be assigned to the non-equivalent ethylammonium cations, nevertheless both the CH_3- and NH_3-groups reorient independently[32] (the C_3-type reorientation) with almost the same correlation times and activation energy E_a (see Table S4†).[33] Quite a weak anomaly on the ^{1}H T_1 *vs.* 1/*T* curve close to 190 K confirms the presence of the PT which is rather close to the continuous one. Just above the PT at 190 K, the E_a value increases significantly up to 19 J mol^{-1} and then gradually decreases. Such a behaviour suggests an onset of a unified axial like motion of whole ethylammonium cations.

The UV-Vis absorption spectra of **ECB** (shown in Fig. 5) were measured at various temperatures (175 K–275 K) to establish how the distortion of an anionic lattice influences the electronic structure of the $[BiCl_6]^{3-}$ moiety. The spectra of the Bi^{3+} ion may be analyzed in terms of either the s → p transitions in the free Bi^{3+} ion or the transitions between the molecular orbitals of the $[BiCl_6]^{3-}$ complex.[34] In general, the UV absorption spectra of simple ns^2 complexes are characterized by the presence of A, B and C bands of the free ns^2 ions, whose energy and intensity depend slightly on the structural changes of the ns^2 complex.[35]

Of these bands, the A band centered at ~340 nm is particularly sensitive to the geometry of the distortion of the *ns*^{2} complex.[36] Indeed, the observed discontinuous changes in the A band maximum as well as its half width in the spectra of **ECB** seem to confirm this conclusion. Taking into account the structural changes, one may conclude that the more rigid structure of the anionic $[BiCl_6]^{3-}$ complex in Phase I becomes less tight in Phase II. This, in turn, probably causes a certain decrease of the energy of the HOMO antibonding a_1 orbital (assuming the C_{2v} symmetry of the $[BiCl_6]^{3-}$ complex in Phase I), which reflects in a hypsochromic shift of the A band maxima by 525 cm^{-1} in the spectrum of Phase II. The half bandwidth decreases by about 650 cm^{-1} on lowering the temperature from 225 K to 175 K.

Conclusions

In conclusion, this paper demonstrates the successful development in the field of ferroelectricity among the organic–inorganic hybrid materials. The newly synthesized bis(ethylammonium) pentachlorobismuthate(III): $(C_2H_5NH_3)_2BiCl_5$ belongs to a unique group of ferroelectrics characterized by the *cis* configuration of the $[MX_5]^{2-}{}_\infty$ chains and P_s equals to 1.4 μC cm^{-2} at 180 K. The molecular mechanism of the ferroelectric PT seems to be related mostly to the distortion of the anionic sublattice, nevertheless the contribution of the organic part (ordering of the ethylammonium cations) is incontestable. For this reason, **ECB** should be classified as a ‘displacive’ ferroelectric.

Experimental

Synthesis of the complex

ECB polycrystals were obtained by dissolving stoichiometric amounts of ethylamine and Bi_2O_3 in a concentrated HCl solution at 320 K. After few days, white solids were formed by a slow evaporation from the colorless solution. The polycrystalline material obtained was recrystallized twice and characterized by an elemental analysis: C: 10.11% (theor. 10.04%), N: 5.72% (theor. 5.86%), H: 3.55% (theor. 3.37%) and IR spectrum (Fig. S1†).

Thermal studies

Differential scanning calorimetry (DSC) runs were recorded using a PerkinElmer DSC-7 in the temperature range 100–300 K with a scanning rate of 10 K min^{-1}. TGA and DTA measurements were performed on a Setaram SETSYS 16/18 instrument in the temperature range 300–700 K with a ramp rate of 2 K min^{-1} (Fig. S2†). The scan was performed under flowing nitrogen (flow rate: 1 dm^3 h^{-1}).

Dielectric studies

Dielectric measurements were performed with a Novocontrol impedance analyzer. The measurements were performed in the frequency range 1 Hz to 1 MHz and over the temperature range from 160 K to 210 K. The alternating electric field of amplitude 1 V was applied across the sample. As the single crystals were not obtained, the powder of well-dried samples was measured instead. The measurement chamber consisted of a quartz ring with a height of 0.44 mm and an inner diameter of 6.65 mm. The electrodes were copper discs of the diameter of 12.83 mm. The powder completely filled the measuring chamber. Gas nitrogen was used to maintain the temperature during the dielectric measurements and the temperature inside the cryostat was controlled by using the Novocontrol Quattro Cryosystem. The temperature stability of the samples was better than 0.01 K. The combined standard uncertainties of data were estimated to be lower than 1% of the measured values.

The spontaneous polarization was measured between 100 and 200 K by a charge integration technique using a Keithley 617 Programmable Electrometer. The temperature was stabilized by using an Instec STC 200 temperature controller. Ferroelectric hysteresis loop measurements were performed using a home-made high precision set-up based on the Diamant–Drenck–Pepinsky (DDP) bridge.

Crystal structure analysis

X-ray diffraction was performed on a Xcalibur, Sapphire2 four-circle diffractometer operating with Mo Kα radiation (λ = 0.7107 Å) and a CCD camera (large Be window). Data were measured in a ω-scan mode with $\Delta\omega = 1.0°$. The CrysAlis CCD and CrysAlis RED were used for data collection and processing.[37] The measurements were performed at room temperature (Phase I) and 100 K (Phase II). The structures were solved by direct methods and refined using full-matrix least-squares methods with SHELXL2014/7. Empirical absorption correction using spherical harmonics, implemented in the SCALE3 ABSPACK scaling algorithm, was applied on all data. In the RT phase, the distance restraints (DFIX) were applied on the C–C and C–N distances to preserve the chemically reasonable geometry of ethylammonium cations which was disturbed by the large, thermally activated atomic displacements. In the low-temperature phase, similar restraints were applied only on disordered ethylammonium cations. Additionally, atomic displacement factors of disordered cations were refined with SIMU and DELU limitations. The details of the data collection and refinement together with the crystal description are given in Table S1.† Table S2† shows the selected interatomic distances.

For both structures: $C_4H_{16}BiCl_5N_2$, M_r = 478.42, Z = 8. **Phase I** (295 K): orthorhombic, *Acam* (non-standard setting of *Cmca*, no. 64). a = 17.8318(2) Å, b = 21.9673(8) Å, c = 7.5656(4); V (Å^3) 2963.57(19); R_{int} 0.043, $R[F^2 > 2\sigma(F^2)]$ 0.027, w$R(F^2)$ 0.069, S 1.12; no. of reflections 2229; no. of parameters 78; no. of restraints 34; $\Delta\rho_{\max}$ 0.86; $\Delta\rho_{\min}$ −0.74. **Phase II** (100 K): orthorhombic, *Aba*2 (no. 41). a = 17.5405(4) Å, b = 21.7670(4) Å, c = 7.4791(2) Å; V (Å^3) 2855.54(10); R_{int} 0.06, $R[F^2 > 2\sigma(F^2)]$ 0.039, w$R(F^2)$ 0.111, S 1.11; no. of reflections 2869; no. of parameters 137; no. of restraints 40; $\Delta\rho_{\max}$ 1.68; $\Delta\rho_{\min}$ −2.17; refined as an inversion twin (absolute structure parameter 0.462 (17)).

NMR measurements

NMR measurements were performed using an ELLAB TEL-Atomic PS 15 spectrometer. Spin–lattice relaxation times T_1 at 25 MHz were measured using a saturation sequence of π/2 pulses followed by a variable time interval τ and a reading π/2 pulse. The magnetization was found to recover exponentially within the experimental error at all temperatures. The temperature of the sample was controlled by using a UNIPAN 660 temperature controller operating on a Pt 100 sensor providing a long time temperature stability better than 1 K. The sample of powdered ethylammonium $BiCl_5$ was evacuated at room temperature and then sealed under vacuum in a glass ampoule. All measurements were performed on heating the sample from liquid nitrogen temperature. The errors in the measurements of T_1 were estimated to be about 5%.

Absorption spectra

The absorption spectra were recorded on a Cary 5000 UV/Vis/NIR. The spectra of the powder in polyethylene pellets were measured at different temperatures (125 K–275 K) in a continuous flow helium cryostat (Optistat, Oxford). The spectra were corrected by subtracting the background of polyethylene pellets.

Acknowledgements

This work was supported by the National Science Centre; grant no. 2013/11/D/ST8/03297 (A. Piecha-Bisiorek).

References

1 M. E. Lines and A. M. Glass, *Principles and Applications of Ferroelectrics and Related Materials*, Oxford University Press, Oxford, U. K., 1991.

2 J. F. Scott, *Ferroelectric Memories*, Springer, Berlin, 2000.

3 Z. G. Ye, *Handbook of advanced dielectric, piezoelectric and ferroelectric materials: Synthesis, properties and applications*, Woodhead Publishing, Cambridge, U. K., 2008.

4 (*a*) J. F. Scott, *Science*, 2007, **315**, 954–959; (*b*) S.-T. Han, Y. Zhou and V. A. L. Roy, *Adv. Mater.*, 2013, **25**, 5425–5449; (*c*) J. Li, J. Claude, L. E. Norena-Franco, S. I. Seok and Q. Wang, *Chem. Mater.*, 2008, **20**, 6304–6306; (*d*) S. Hong, O. Auciello and D. Wouters, *Emerging Non-Volatile Memories*, Springer US, 2014.

5 W. P. Zhao, C. Shi, A. Stroppa, D. Di Sante, F. Cimpoesu and W. Zhang, *Inorg. Chem.*, 2016, **55**, 10337–10342.

6 W. Bi, N. Leblanc, N. Mercier, P. Auban-Senzier and C. Pasquier, *Chem. Mater.*, 2009, **21**, 4099–4101.

7 N. Leblanc, N. Mercier, L. Zorina, S. Simonov, P. Auban-Senzier and C. Pasquier, *J. Am. Chem. Soc.*, 2011, **133**, 14924–14927.

8 N. Leblanc, N. Mercier, M. Allain, O. Toma, P. Auban-Senzier and C. Pasquier, *J. Solid State Chem.*, 2012, **195**, 140–148.

9 M. Owczarek, P. Szklarz, R. Jakubas and A. Miniewicz, *Dalton Trans.*, 2012, **41**, 7285–7294.

10 A. Piecha, A. Białońska and R. Jakubas, *J. Mater. Chem.*, 2012, **22**, 333–336.

11 K. Eckhardt, V. Bon, J. Getzschmann, J. Grothe, F. M. Wisser and S. Kaskel, *Chem. Commun.*, 2016, **52**, 3058–3060.

12 G. Xu, Y. Li, W.-W. Zhou, G.-J. Wang, X.-F. Long, L.-Z. Cai, M.-S. Wang, G.-C. Guo, J.-S. Huang, G. Bator and R. Jakubas, *J. Mater. Chem.*, 2009, **19**, 2179–2183.

13 L. Sobczyk, R. Jakubas and J. Zaleski, *Pol. J. Chem.*, 1997, **71**, 265–300.

14 W. Zhang and R.-G. Xiong, *Chem. Rev.*, 2012, **112**, 1163–1195.

15 R. Jakubas, U. Krzewska, G. Bator and L. Sobczyk, *Ferroelectrics*, 1988, **77**, 129–135.

16 R. Jakubas, Z. Galewski, L. Sobczyk and J. Matuszewski, *J. Phys. C: Solid State Phys.*, 1985, **18**, L857–L860.

17 J. Mróz and R. Jakubas, *Ferroelectrics Lett.*, 1994, **17**, 73–78.

18 M. Iwata, *J. Phys. Soc. Jpn.*, 1993, **62**, 3315–3326.

19 J. Zaleski and A. Pietraszko, *Acta Crystallogr., Sect. B: Struct. Sci.*, 1996, **52**, 287–295.

20 R. Jakubas, *Solid State Commun.*, 1986, **60**, 389–391.

21 R. Jakubas, L. Sobczyk and J. Matuszewski, *Ferroelectrics*, 1987, **74**, 339–345.

22 G. Bator, R. Jakubas, L. Sobczyk and J. Mróz, *Ferroelectrics*, 1993, **141**, 177–187.

23 M. Bujak and J. Zaleski, *Cryst. Eng.*, 2001, **4**, 241–243.

24 P. Carpentier, L. Lefebvre and R. Jakubas, *Acta Crystallogr., Sect. B: Struct. Sci.*, 1991, **47**, 228–234.

25 R. Jakubas, *Solid State Commun.*, 1989, **69**, 267–269.

26 J. Józków, R. Jakubas, G. Bator and A. Pietraszko, *J. Chem. Phys.*, 2001, **114**, 7239–7246.

27 A. Piecha, A. Pietraszko, G. Bator and R. Jakubas, *J. Solid State Chem.*, 2008, **118**, 1155–1166.

28 A. Piecha, A. Białońska and R. Jakubas, *J. Phys.: Condens. Matter*, 2008, **20**, 1–9.

29 R. Jakubas, A. Piecha, A. Pietraszko and G. Bator, *Phys. Rev. B: Condens. Matter*, 2005, **72**, 1–8.

30 J. Laane and P. W. Jagodzinsky, *Inorg. Chem.*, 1980, **19**, 44–49.

31 D. Orobengoa, C. Capillas, M. I. Aroyo and J. M. Perez-Mato, *J. Appl. Crystallogr.*, 2009, **A42**, 820–833.

32 H. Ishida, N. Kumaga and S. Sato, *Z. Naturforsch., A: Phys. Sci.*, 2001, **56**, 523–526.

33 H. Terao, Y. Furukawa, M. Hashimoto, K. Yamada and T. Okuda, *Z. Naturforsch., A: Phys. Sci.*, 2002, **57**, 369–374.

34 (*a*) A. Vogler and H. Nikol, *Comments Inorg. Chem.*, 1993, **4**, 245–261; (*b*) T. A. Albright, J. K. Burdett and M.-H. Whangbo, *Orbital Interactions in Chemistry*, Willey, 2013.

35 (*a*) A. Vogler, A. Paukner and H. Kunkely, *Coord. Chem. Rev.*, 1990, **97**, 285–297; (*b*) G. Blasse, *Electronic and Vibronic Spectra of Transition Metal Complexes I in Topics in Current Chemistry*, ed. H. Yersin, 1994, vol. 171, p. 1.

36 M. Wojciechowska, P. Szklarz, A. Białońska, J. Baran, R. Janicki, W. Medycki, P. Durlak, A. Piecha-Bisiorek and R. Jakubas, *CystEngComm*, 2016, **18**, 6184–6194.

37 CrysAlis CCD, CrysAlis RED Oxford Diffraction Ltd., Version 1.171.33.66 (release 28-04-2010 CrysAlis171.NET) (compiled Apr 28 2010, 14:27:37).